Decomposition of the Precursor $[Pt(NH_3)_4](OH)_2$, Genesis and Structure of the Metal−Support Interface of Alumina Supported Platinum Particles: A Structural Study Using TPR, MS, and XAFS Spectroscopy

A. Muñoz-Páez[†] and D. C. Koningsberger*[,‡]

Department of Inorganic Chemistry, University of Sevilla, P.O. Box 553, 41012 Sevilla, Spain, and Laboratory of Inorganic Chemistry and Catalysis, Debye Institute, University of Utrecht, P.O. Box 80083, 3508 TB Utrecht, The Netherlands

Received: August 15, 1994; In Final Form: January 3, 1995[⊗]

During the preparation of alumina supported platinum catalysts, the precursor $[Pt(NH_3)_4](OH)_2$ decomposes to a neutral $Pt(NH_3)_2O$ species during the drying process at 120 °C. Treatment in flowing hydrogen at 180 °C leads to partial reduction of the platinum ammine complex and formation of platinum metal particles. A large increase in metal particle size is observed after a treatment under flowing H_2 at 200 °C. The final reduction at 350 °C causes the total disappearance of the platinum precursor with a further increase in platinum particle size. The direct reduction at 350 °C yields the biggest metal particles (35 Å) while calcination before reduction produces a much higher dispersion (metal particle diameter 10 Å). The beneficial effect of calcination, already observed by many authors when using $[Pt(NH_3)_4](OH)_2$ as a precursor for the preparation of highly dispersed Pt/γ-Al_2O_3, can now be explained because this treatment avoids the formation of the mobile neutral $Pt(NH_3)_2O$ complex. The metal particles produced by treatment in flowing hydrogen at 180 °C present a metal−oxygen contribution at 2.7 Å formed at the metal−support interface. This long distance is assumed to be caused by the presence of hydrogen in the metal−support interface based upon our results in combination with other TPD and EXAFS studies. A second metal−oxygen contribution with similar coordination number is detected at 3.86 Å. This is a consequence of the presence of the first shell metal−oxygen at 2.7 Å and implies a [111] epitaxy in the metal−support interface.

Introduction

Supported metal catalysts are generally prepared by impregnation of the support with an aqueous solution containing the metallic precursors. Subsequent drying and/or calcination followed by reduction with hydrogen leads to the catalytic active phase.[1] Although all these steps strongly influence the final properties of the catalyst and, hence, its performance under reaction conditions, attention has been focused only on the influence of high temperature treatments under oxygen and/or hydrogen on the final metal particle shape and size. Among supported metal catalysts Pt/γ-Al_2O_3 is one of the most studied because it is widely used as a reforming and cracking catalyst. The influence of oxidation and reduction treatments on this system has been studied with TPR/TPD,[2,3] IR,[4] XPS,[5] TEM,[6] and XAFS spectroscopy.[7−9] The structural and electronic properties of platinum particles dispersed in zeolites have also been investigated recently with XAFS spectroscopy.[10−14]

Recent results have demonstrated the important role of the initial steps in the preparation procedure on the agglomeration of the metal particles. Ardiles et al. have shown that the impregnation step is crucial when the species to be deposited shows a strong interaction with the support, while the drying step has a marked influence on the final properties of the catalyst when the interaction between the precursor and the support is weak.[15,16] It should be realized that uptake of transition metal complexes by oxide surfaces can be associated with a ligand exchange reaction between a surface hydroxyl group and a ligand of the metal complex, incorporating the surface ligands into the complex.[17] The chemical behavior of the metal precursor complex can give hints for understanding the processes taking place during the chemical reaction of the precursor complex with the surface. Another important issue is the influence of water vapor pressure during the reduction of the metallic precursor.[18] A high water vapor pressure favors the increase of the metal particle size.

Characterization studies of the Pt/A_2O_3 catalyst at the initial stage of preparation (i.e., impregnation and drying) are not as abundant as the studies of the effect of the final high temperature treatment in oxygen and/or hydrogen. The metal precursor compounds which are commonly used contain chlorine ligands. They provide good metal dispersions, both by the decomposition of the complex and by formation of oxochloro compounds.[19] Moreover, chlorine modifies the acidity of the support, improving the catalytic performance in naphtha reforming processes.[20] Nevertheless, there are several processes in which chlorine hampers the catalytic activity of the system.[21] In this case the use of another Pt precursor is strongly recommended since once chlorine reacts with the support, it is very difficult to remove it, because it can be included in the support network.[22]

Among the possible alternatives, $[Pt(NH_3)_4](OH)_2$ is one of the most attractive since the residual product (ammonia) can be removed from the surface of the support by heating under inert atmospheres. The use of platinum ammine complexes is crucial for the preparation of highly dispersed platinum particles in zeolite, used for several reforming reactions (*n*-hexane dehydrocyclization, benzene hydrogenation.) Dalla Betta and Boudart in 1972[23] found that calcination of a Pt/Y sample prepared using $[Pt(NH_3)_4](OH)_2$ resulted in a high metal dispersion. However, Pt/L zeolite supported catalysts can be prepared with a high dispersion by direct reduction in hydrogen of the ammine precursor,[14] while calcination before reduction

* To whom correspondence should be addressed.
[†] University of Sevilla.
[‡] University of Utrecht.
[⊗] Abstract published in *Advance ACS Abstracts,* March 1, 1995.

0022-3654/95/2099-4193$09.00/0

at temperatures higher than 300 °C leads to large particles outside the zeolite channels.[24] In contrast with the abundant information obtained for the H_2PtCl_6 precursor,[9,18,19] there is a gap in the knowledge of the activation process of the platinum–ammine precursor.

A combination of TPD (temperature programmed desorption) and EXAFS measurements carried out on the Pt/K-LTL catalytic system[13,14] has demonstrated that the structure of the metal–zeolite interface is dependent on the reduction treatment in hydrogen. LTR (low temperature reduction ~300 °C) leads to the presence of hydrogen in the metal–zeolite interface resulting in a metal–oxygen coordination around 2.7 Å. HTR (high temperature reduction ~600 °C) gives metal–oxygen bonds around 2.2 Å, whereas at intermediate reduction temperatures bometal–supportth types of metal–oxygen coordinations are detected. For Pt/γ-Al_2O_3 catalysts detailed information about the structure and epitaxy in the metal–support interface and their dependence on the reduction temperature is lacking.

In this study a combination of TPR (temperature programmed reduction), MS, and XAFS (X-ray aborption fine structure) spectroscopy is used to follow the initial stages of decomposition of $[Pt(NH_3)_4](OH)_2$ onto Al_2O_3 under inert and reducing atmospheres. The final goal of this paper is to determine the first stages of the metal–metal bond and metal–support interface formation. Attention has been focused onto four main aspects: (i) identification of the platinum entities undergoing reduction, (ii) determination of the threshold of metal–metal bond formation, (iii) study of the formation of the metal–support interface, and (iv) study of the influence of the pretreatment (calcination and reduction vs direct reduction and, in both cases, reduction temperature) on the structure of the platinum metal particles and on the metal–support interface.

Experimental Section

A 1 wt % Pt/γ-Al_2O_3 (sample 1) catalyst was prepared by incipient wetness of a γ-Al_2O_3 support, Ketjen CK-300 with a superficial area of 200 m^2/g and 0.56 mL/g pore volume, with a known amount of $[Pt(NH_3)_4](OH)_2$, from Strem Chemical Newburyport, dried at 120 °C for 15 h, and stored in air. This sample was submitted to several decomposition treatments under inert and reducing atmospheres and its evolution followed with the techniques described below.

To check the effect of calcination treatments on the final metal dispersions, another Pt/γ-Al_2O_3 catalyst (sample 2) was prepared in a similar way, but instead of drying it under He before reducing, it was calcined in air at 350 °C and reduced at the same temperature. In this sample only the EXAFS spectrum of the reduced system has been recorded.

Temperature programmed reduction experiments were carried out with a conventional TCD system connected to an HP-3054-DL system for data storage and processing. A gas stream (5% H_2 in Ar, 10 mL/min) was passed through the sample using a constant heating rate of 10 °C/min. The TC detector for hydrogen consumption was calibrated with CuO being linear in a range of 10–200 μmol. The total hydrogen uptake was obtained by integration of the area under the curve. No hydrogen consumption was detected in the range 25 to 600 °C in the bare support.

Mass spectra were recorded in a flow system connected to a quadrupole mass spectrometer (QMS), PGA-100, that allows the recording of eight different signals per second. The system is controlled by a PC that also stores the data.

EXAFS measurements of the catalysts were performed at EXAFS station 9.2 of the Wiggler beam line of the SRS at Daresbury (U.K.). This station is operating with a double crystal monochromator Si[220], which was detuned to 50% intensity to minimize the presence of higher harmonics. The estimated resolution was 3 eV at the Pt L_{III} edge (11 564 eV). The measurements were carried out in transmission mode using optimized ion chambers as detectors. Each data point was collected for 1 s, and at least two to four scans were averaged, thus minimizing high- and low-frequency noise.

TABLE 1: Crystallographic Data and Fourier Filtering Ranges of Reference Compounds

compound	Ab–Sc pair	k^n	FT range ($Å^{-1}$)	filter range (Å)	N	R (Å)	ref
Pt foil	Pt–Pt	3	2.2–20.4	1.4–3.1	12	2.77	28
$Na_2Pt(OH)_6$	Pt–O	1	1.8–14.5	0.0–2.3	6	2.05	29
$[Pt(NH_4)_4](OH)_2$	Pt–N	1	1.6–12.5	0.3–2.2	4	2.04	28

The samples were pressed into thin self-supporting wafers with an absorbance of approximately 2.5 and mounted in an in-situ EXAFS cell.[25] EXAFS measurements were done under a controlled atmosphere (He or H_2) on the Pt L_{III} edge at liquid nitrogen temperature. The EXAFS spectra of Pt foil and $Na_2Pt(OH)_6$ were used as references to calculate phase shifts and backscattering amplitude functions of the Pt–Pt and Pt–O absorber–backscatter pair. A water solution of $[Pt(NH_3)_4](OH)_2$ was measured at room temperature, and the EXAFS spectrum was used as a reference to calculate phase shifts and backscattering amplitude functions for Pt–N contribution.

Standard procedures were used to extract the EXAFS data from the measured absorption spectrum. Normalization was done by dividing by the height of the absorption edge, and the background was subtracted using cubic spline routines.[26,27]

The data analysis procedures used to obtain the reference data for Pt foil and $Na_2Pt(OH)_6$ are extensively described in ref 10. The manufacture of the reference functions from EXAFS data of Pt foil, $Na_2Pt(OH)_6$, and $[Pt(NH_3)_4](OH)_2$ is straightforward, since the first shell peak (Pt–Pt, Pt–O, and Pt–N, respectively) in r space shows no overlap with higher shells. The crystallographic first-shell coordination parameters for all the reference compounds, the weighting of the Fourier transform, and the ranges in k and r space used to extract the reference functions from the experimental EXAFS data are given in Table 1.

The EXAFS data analysis was performed using the experimentally determined phase shifts and backscattering amplitudes for the various contributions. To determine reliably the parameters characterizing the high Z (Pt) and low Z (O and N) contributions, multiple shell fitting in k space with subsequent control in r space was done with application of both k^1 and k^3 weighting. The use of both k^1 and k^3 weighting is a prerequisite since the k-dependence of the backscattering amplitude of low Z elements (O and N) is different from that of high Z elements (Pt). The backscattering amplitude of the low Z elements becomes very small above $k = 10$ $Å^{-1}$, in comparison with the amplitude of high Z scatterers, which is still significant at higher k values.[30] Application of only k^3 weighting in systems containing both high and low Z scatterers leads to an underestimation of the contribution of the low Z elements. Moreover, optimizing k^1 and k^3 fits both in k and in r space results in a better decoupling of N (coordination number) and $\Delta\sigma^2$ (Debye–Waller factor) as well as R (coordination distance) and ΔE_0 (inner potential correction) and, therefore, in a more reliable set of parameters.[10] The difference file technique was applied together with phase-corrected Fourier transforms to resolve the different contributions in the EXAFS data.[31]

Due to curved wave effects the phase shift and backscattering amplitude functions obtained from reference compounds are correct only when there is no difference in distance between

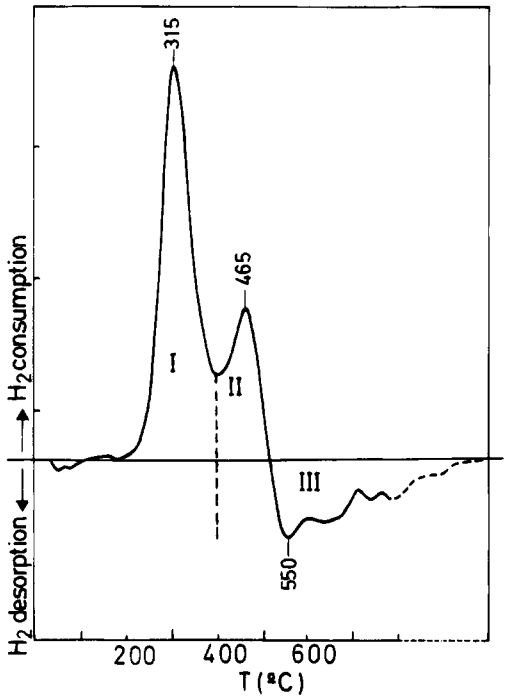

Figure 1. TPR profile of $[Pt(NH_3)_4](OH)_2/\gamma\text{-}Al_2O_3$ sample after impregnation and drying.

the reference compound and the unknown. Thus, coordination numbers need to be corrected for a difference in distance between the reference compound and the unknown according to[10]

$$N_{cor} = N \exp[-2(R_{ref} - R_{fit})/\lambda]$$

The errors in the structural parameters were calculated from the covariance matrix taking into account the statistical noise of the EXAFS data and the correlations between the different coordination parameters.[32] We have not found a simple function to evaluate systematic errors, so they are not included in the calculation of the standard deviations. The amplitude of the noise was estimated from the raw data at those k values, where the EXAFS signal was sufficiently damped out. The values of the goodness of fit (ϵ_ν^2) were calculated as outlined in the Reports on Standard and Criteria in XAFS Spectroscopy.[33]

Results

Temperature Programmed Reduction Profiles. The TPR profile of sample 1 (submitted first to a drying treatment under Ar flow up to 200 °C for 1 h) shows two hydrogen-consuming processes (peaks I and II in Figure 1) peaking at 315 and 465 °C, respectively. A desorption process (peak III in Figure 1) is maximum around 550 °C. The hydrogen uptake is $H_2/Pt = 0.85$ in the first process and $H_2/Pt = 0.32$ in the second process. The hydrogen desorption is $H_2/Pt = 0.43$ in the third (negative) peak. The overall hydrogen consumption (I + II − III) is $H_2/Pt = 0.75$.

It has to be pointed out that the abnormally high temperatures of the maxima in H_2 consumption and desorption are due to the extreme experimental conditions used to get the maximum sensitivity with the minimum amount of sample (H_2/Ar flow = 10 mL/min). This causes a linear shift of around 50 °C in the absolute position of the maxima. In fact, in preliminary measurements carried out with standard conditions (50 mL/min, larger of amount of sample) the maxima in the TPR profiles were shifted 65 °C toward lower temperatures.

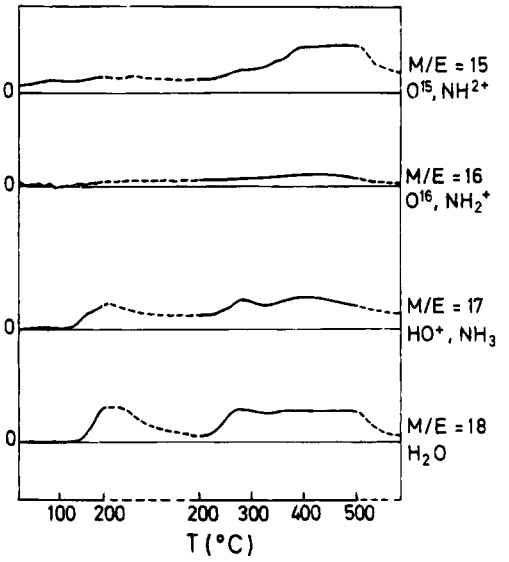

Figure 2. Mass spectra of $[Pt(NH_3)_4](OH)_2/\gamma\text{-}Al_2O_3$ sample after impregnation and drying. Profiles recorded during the decomposition process under H_2 for signal with *m/e* ratio 18 (H_2O), 17 (HO^+, NH_3), 16 (^{16}O, NH^+_2), and 15 (^{15}O, NH^{2+}).

Mass Spectroscopy. To gain additional information about the decomposition of the $[Pt(NH_3)_4](OH)_2$ complex, especially about the evolution of ammonia, the mass spectra of sample 1 submitted to thermal treatment under H_2 at increasing temperatures have been recorded. The results are shown in Figure 2, where the evolution of the species with m/e = 18, 17, 16, 15 (m/e is mass to charge ratio) has been plotted against temperature. The identification of NH_3 (m/e = 17) in the presence of water is quite difficult since both OH^+ and NH_3 have the same m/e (=17). Moreover, ^{16}O and NH_2^+ both have m/e = 16. Thus, the production of four species has to be followed in order to study the decomposition of the platinum ammine complex present on the surface. The species with m/e = 17 and 18 give information about the evolution of water and the species with m/e = 15 and 16, about the evolution of ammonia. The maxima appearing at 200 °C and between 250 and 500 °C in the signal with m/e 18 can be ascribed to the dehydration and dehydroxylation processes of the alumina surface, respectively.[34] The same two processes dominate the signal with m/e = 17, and hardly any changes are recorded in the signal with m/e = 16. The signal with m/e = 15 shows a new process starting at about 300 °C and reaching a maximum at 400 °C. This process can be attributed to ammonia evolution, according to previous studies of ammonia desorption from modified alumina.[35]

X-ray Absorption Fine Structure Spectroscopy (XAFS). *1. Experimental Conditions.* X-ray absorption spectra have been recorded at four stages of the decomposition of the platinum ammine complex in sample 1 under inert/reducing atmospheres. The first spectrum has been recorded under He after submitting the sample to a drying treatment under He flow at 120 °C for 15 min, heating rate of 5 °C/min (designated as sample HE120). This treatment was given to the sample in order to remove physisorbed water, thus preventing the sintering of the metal particles during the subsequent reduction process.[18] Additionally, it provides a well-defined state of the system before the reduction process is carried out.

The activation in hydrogen was followed by recording the EXAFS spectra with the sample exposed to 1 atm of H_2 after reduction at three different temperatures. The second spectrum was recorded at the beginning of the reduction process, with treatment with H_2 at 180 °C for 20 min, heating rate of 5 °C/min (designated as sample DECH180). The third spectrum was

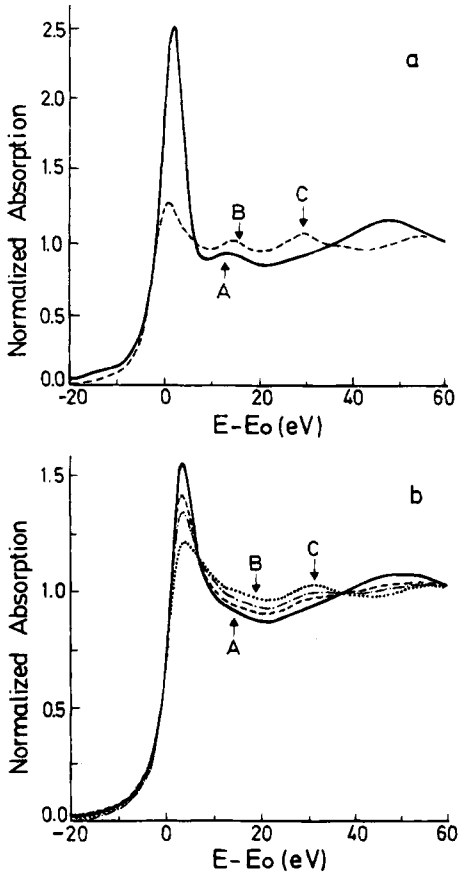

Figure 3. (a) Pt L_{III} edge of platinum tetraammine complex (solid line) and platinum foil (dashed line). (b) Pt L_{III} edge of samples HE120 (solid line), DECH180 (dashed line), DECH200 (dashed-dotted line), and DECH350 (dotted line).

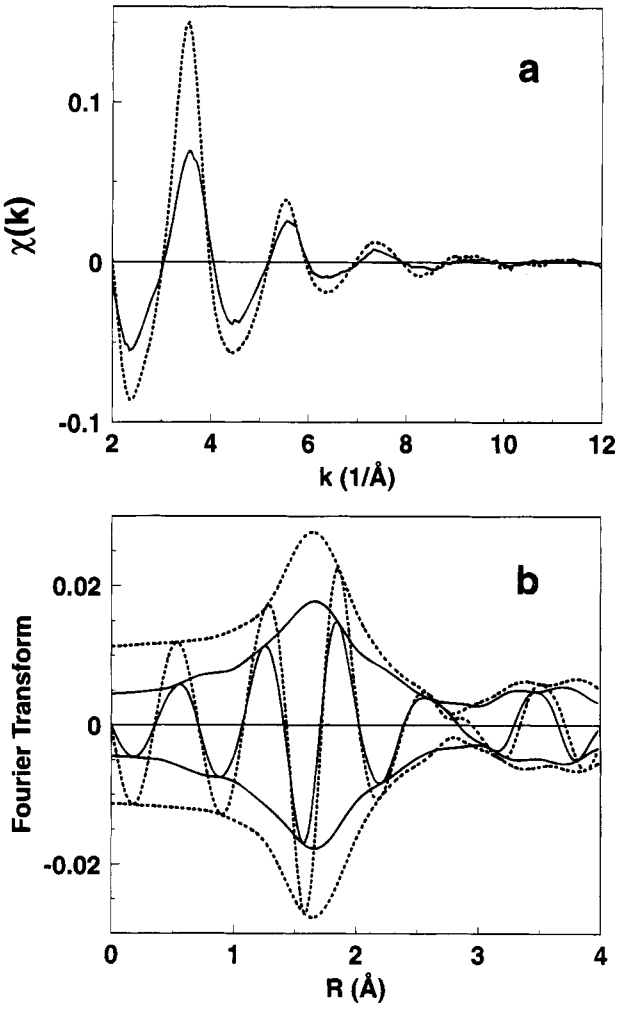

Figure 4. (a) EXAFS raw data of water solution of $[Pt(NH_3)_4](OH)_2$ (dotted line) and of sample HE120 (solid line). (b) k^1-weighed Pt–N phase-corrected Fourier transform of EXAFS spectrum of sample HE120 [Δk = 3.0 – 11.6 Å^{-1}] (solid line) and $[Pt(NH_3)_4](OH)_2$ [Δk = 3.0 – 12.3 Å^{-1}] (dotted line).

measured after a further reduction in H_2 at 200 °C for 20 min, heating rate of 5 °C/min (designated as sample DECH200). The choice of both temperatures was not obvious because a direct extrapolation of the peak positions in the TPR system cannot be made. The absolute position of the TPR peaks has to be corrected by −65 °C, as described above. With this correction it can be seen that at 180 °C, just at the beginning of the reduction process, it has gone far enough to produce detectable amounts of platinum particles but with a reasonable fraction of the dried precursor still present. The temperature of 200 °C was chosen to establish an intermediate situation during the reduction process. The temperature of the fourth treatment (heating rate of 5 °C/min, 350 °C for 30 min) (sample DECH350) resulted in a fully reduced sample (H_2/M = 0.85, where M = metal).

To study the influence of a "normal" reduction treatment (no slow decomposition, i.e., direct heating in H_2 from room temperature to 350 °C with a rate of 5 °C/min, 1 h at 350 °C), another spectrum (sample R350) has been recorded in sample 1. To determine the influence of calcination prior to the reduction treatment, sample 2 (calcined after impregnation) was reduced in flowing H_2 (heating rate 5 °C/min from room temperature to 350 °C, 1 h at 350 °C). The EXAFS spectrum obtained from this sample is indicated by sample OR350.

2. XANES. To follow the decomposition of the adsorbed platinum species and the formation of the Pt–Pt bonds, the white line of the Pt L_{III} edge has been recorded for sample 1. Figure 3a includes the normalized XANES spectra of the Pt L_{III} X-ray absorption edge of the $[Pt(NH_3)_4](OH)_2$ complex (solid line) and Pt foil (dashed line). These spectra have been plotted vs $E - E_0$ (total energy minus edge energy) with this last value being defined as the major inflection point in the edge. The difference in amplitude of the threshold peak (white line) is caused by the difference in oxidation state (Pt^{2+} vs Pt^0). A characteristic feature in the shape of the XANES spectrum of the platinum ammine complex is the peak at 13 eV after the absorption edge (peak A in Figure 3a). The XANES spectrum of Pt foil can be identified by peak B (15 eV) and peak C (30 eV).

Figure 3b presents the XANES spectra of the HE120 (solid line), DECH180 (dashed line), DECH200 (dotted-dashed line), and DECH350 (dotted line). The high amplitude of the white line and the presence of peak A in the XANES spectrum of the HE120 sample point to the existence of Pt–N bonds in the adsorbed platinum species. The continuous decrease in the intensity of the white line induced by treatment under hydrogen at increasing temperatures indicates a progressive reduction of Pt^{2+} ions. Also the disappearance of peak A characteristic of the presence of Pt–N bonds shows the decomposition of the platinum complex. The presence of peaks B and C in the sample DECH350 is an indication of the formation of platinum metal particles.

3. EXAFS. The raw EXAFS spectra of the $[Pt(NH_3)_4](OH)_2$ complex and the HE120 sample are displayed in Figure 4a. A comparison of both spectra shows the similarity in nodes and shape. However, the amplitude of the EXAFS oscillations at low k values is smaller for the HE120 sample, and there is a

TABLE 2: Fourier Filtering and Analysis Ranges

sample	FT weight k^n	FT range Δk (Å^{-1})	filter range ΔR (Å)	fit weight k^n	analysis range Δk (Å^{-1})	N_{indp}[a]	ν[b]	amplitude noise	ϵ_ν^{2} [b,c]
HE120			(0.0−4.0)[d]	0	3.5−12.0	22.6	14.6	0.002	2.05
DECH180	1	2.9−13.1	0.1−4.1	1	3.5−12.5	23.9	7.9	0.002	0.52
DECH200	1	2.1−12.0	0.5−4.2	1	3.5−11.5	20.3	8.3	0.0015	1.09
DECH350	3	2.6−12.1	0.9−6.3	2	3.0−11.0	28.5	12.5	0.003	0.74
R350	2	2.7−16.7	1.1−5.9	2	3.5−16.0	39.2	23.2	0.002	1.61
OR350	2	2.6−14.3	1.0−4.1	1	3.5−13.5	20.7	4.7	0.001	1.60

[a] N_{indp} is number of independent parameters; $N_{indp} = 2\Delta k\Delta R/\pi + 1$. [b] ν is degrees of freedom; $\nu = N_{indp} - N_{fit}$. [c] See Report on Standards and Criteria.[33] [d] Range in r space used to fit the unfiltered EXAFS.

clear difference in node position for $k = 4.1$ Å^{-1}. This is an indication of a decrease in Pt−N coordination after adsorption of the ammine complex onto the support and the occurrence of a new type of bond. This can be seen more clearly in Figure 4b, which includes the magnitude and imaginary part of the k^1-weighted Fourier transform (corrected for the Pt−N phase, thus emphasizing the Pt−N contribution). An inspection of the imaginary part also reveals differences in positions of nodes between $1 < R < 2$ Å.

Two structural models have been tried to fit the raw EXAFS spectrum (noise level is estimated to be 0.002). The number of independent points N_{indp} in the spectrum calculated according to the Nyquist theorem[32] for the fitting range ($\Delta k = 3.5-12$ Å^{-1}, $\Delta R = 0-4$ Å) amounts to 22.6 (see also Table 2). A model with one Pt−N coordination ($N_{fit} = 4$ with $\nu = 18.6$ degrees of freedom) gives a goodness of fit value $\epsilon_\nu^2 = 5.2$, with $N = 2$ for the coordination number and $R = 2.03$ Å for the coordination distance. Introducing also a coordination with oxygen ($N_{fit} = 8$ with $\nu = 14.6$ degrees of freedom) leads to the coordination parameters as presented in Table 3. This model describes the data with a goodness of fit value $\epsilon_\nu^2 = 2.05$. The confidence limit of the extra Pt−O coordination is calculated to be 96%, which implies that the model with both a Pt−N and a Pt−O coordination describes the data best. It has to be pointed out that Pt−O and Pt−N phase shift and backscattering amplitude functions have been used to fit Pt^{2+}−O and Pt^{2+}−N bonds, respectively. Transferability of these functions among nearest and even next-nearest neighboring elements in the whole periodic table is generally assumed. However, it has been recently shown that the backscattering amplitude function is not transferable for the next-nearest neighbors carbon and oxygen.[36] Small differences are observed between the experimentally obtained nearest neighbor Pt−N and Pt−O backscattering amplitudes (see Figure 5b). Also small but significant differences are detected between the experimentally obtained nearest neighbors phase shift functions, as can be observed in Figure 5a. There is a difference of more than 2π radians which is also dependent on k. These functions have been obtained from the EXAFS data of the $[Pt(NH_3)_4](OH)_2$ and $Na_2Pt(OH)_6$ reference compounds, using the following equations:

$$\chi(k) = A(k)_{exptal} \sin[\phi(k)_{exptal}]$$

phase shift function:

$$\varphi(k) = \phi(k)_{exptal} - 2kR$$

backscattering amplitude function:

$$F(k) = A(k)_{exptal} kR^2/S_0^2 \exp[2R/\lambda] \exp[2\sigma^2k^2]$$

where $A(k)_{exptal}$ is the amplitude function and $\phi(k)_{exptal}$ is the argument of the sine function, obtained by first shell Fourier filtering of experimental data. The functions $\varphi(k)$ and $F(k)$ are obtained using the following input parameters for Pt−N, $N = 4$, $R = 2.04$ Å, $\sigma = 0$, $\lambda = 10$, $S_0^2 = 1$, and for Pt−O, $N = 6$, $R = 2.05$ Å, $\sigma = 0$, $\lambda = 10$, $S_0^2 = 1$. The difference in phase shift data explains why in a statistical analysis a structural model with both a Pt−N and a Pt−O coordination can be distinguished from a model with only one Pt−N shell.

TABLE 3: EXAFS Coordination Parameters[a]

parameters	N	$\Delta\sigma^2$(Å^2) × 10^3	R (Å)	ΔE_0 (eV)
		coordination Pt^{2+}−N		
HE120	2.0 (0.3)	1.0 (1.0)	2.03 (0.01)	2.0 (2.9)
DECH180	1.9 (0.2)	4.6 (1.0)	1.97 (0.01)	8.6 (1.2)
DECH200	1.0 (0.1)	2.2 (1.8)	2.00 (0.01)	3.0 (1.4)
		coordination Pt^{2+}−O		
HE120	1.0 (0.6)	3.9 (0.6)	2.00 (0.02)	9.5 (8.4)
		coordination Pt−O_s		
OR350	0.4 (0.1)	4.0 (6.0)	2.16 (0.03)	−6.5 (5.0)
		coordination Pt−O_{L1}		
DECH180	0.9 (0.6)	−2.4 (8.4)	2.70 (0.06)	−2.7 (6.3)
OR350	0.5 (0.3)	7.0 (10)	2.66 (0.06)	7.0 (7.4)
		coordination Pt−O_{L2}		
DECH180	1.2 (0.3)	−1.3 (3.2)	3.84 (0.03)	−6.8 (1.6)
		coordination Pt−Pt_1		
DECH180	2.5 (1.9)	4.1 (5.5)	2.770[b]	5.3[b]
DECH200	5.2 (0.3)	4.0 (0.6)	2.770 (0.004)	4.2 (0.6)
DECH350	7.2 (0.3)	3.0 (0.5)	2.770 (0.004)	3.3 (0.4)
R350	10.1 (0.2)	2.0 (0.1)	2.771 (0.001)	3.8 (0.2)
OR350	5.5 (0.3)	3.0 (0.3)	2.775 (0.003)	2.5 (0.5)
		coordination Pt−Pt_2		
DECH180	1.5 (0.5)	4.0 (3.5)	3.94[b]	−1.3[b]
DECH200	2.0 (0.4)	4.0 (3.2)	3.95 (0.02)	−6.7 (1.4)
DECH350	2.8 (1.5)	5.7 (6.7)	3.90 (0.04)	−4.3 (3.1)
R350	4.4 (0.5)	2.4 (1.1)	3.93 (0.01)	−5.0 (1.0)
OR350	2.0 (0.3)	3.0 (1.3)	3.96 (0.01)	−8.5 (0.7)
		coordination Pt−Pt_3		
DECH350	8.8 (3.6)	8.2 (6.5)	4.79 (0.04)	1.0 (2.4)
R350	17.5 (1.1)	2.8 (0.6)	4.78 (0.006)	3.3 (0.6)
		coordination Pt−Pt_4		
DECH350	2.4 (1.3)	2.2 (5.2)	5.52 (0.03)	1.9 (1.7)
R350	11.1 (1.0)	4.0 (0.8)	5.52 (0.006)	2.1 (0.4)

[a] Standard deviations were calculated from the covariance matrix and the estimates of the noise level in the scans. [b] Standard deviation not calculated (see text).

The raw EXAFS spectra of the DECH180, DECH200, and DECH350 samples are given in Figure 6a. The decrease of the amplitude around $k = 3.8$ Å^{-1} (characteristic for Pt−N), the progressive increase of the amplitude around $k = 3$ Å^{-1} (characteristic for Pt−Pt), the change in shape of the amplitude, and the difference in nodes are indicative of the formation of platinum metal particles. The magnitude of the k^3-weighted (emphasizing the Pt−Pt contribution) Fourier transform of the raw data is plotted in Figure 6b. This Fourier transform has been corrected for the Pt−Pt phase shift and backscattering amplitude, giving single symmetric peaks at the actual coordination distance. Figure 6b shows the presence of the Pt−Pt bonds (Pt−Pt_1 at 2.77 Å) in the DECH180 sample. A further increase in metal particle size at higher reduction temperatures (samples DECH200 and DECH350) is indicated by the presence of peaks

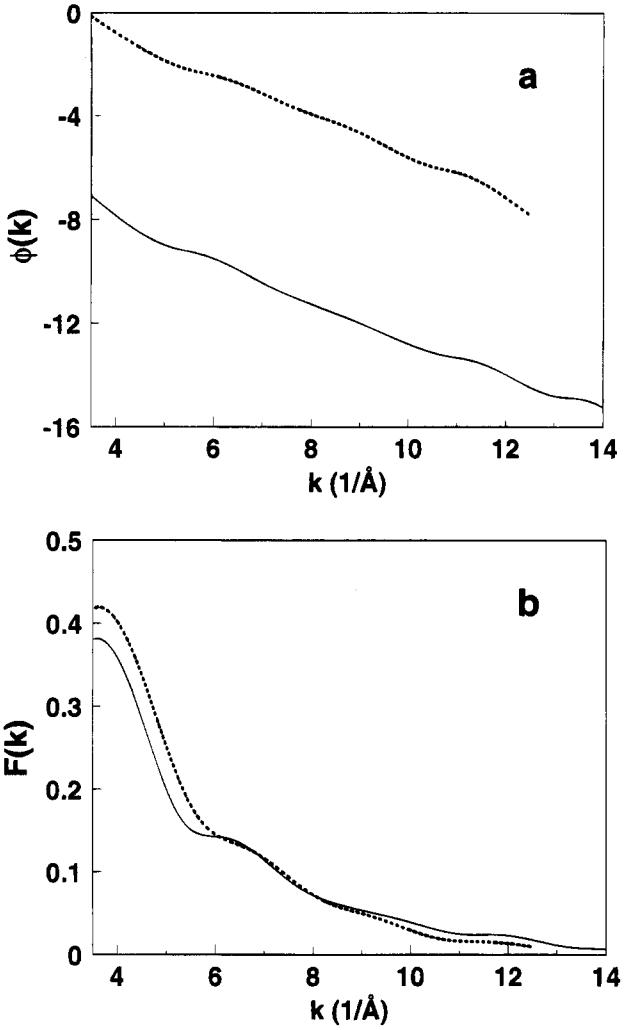

Figure 5. (a) Phase shift function ($\varphi(k)$ and (b) backscattering amplitude function ($F(k)$) Pt−N (solid line) and Pt−O (dashed line) bonds.

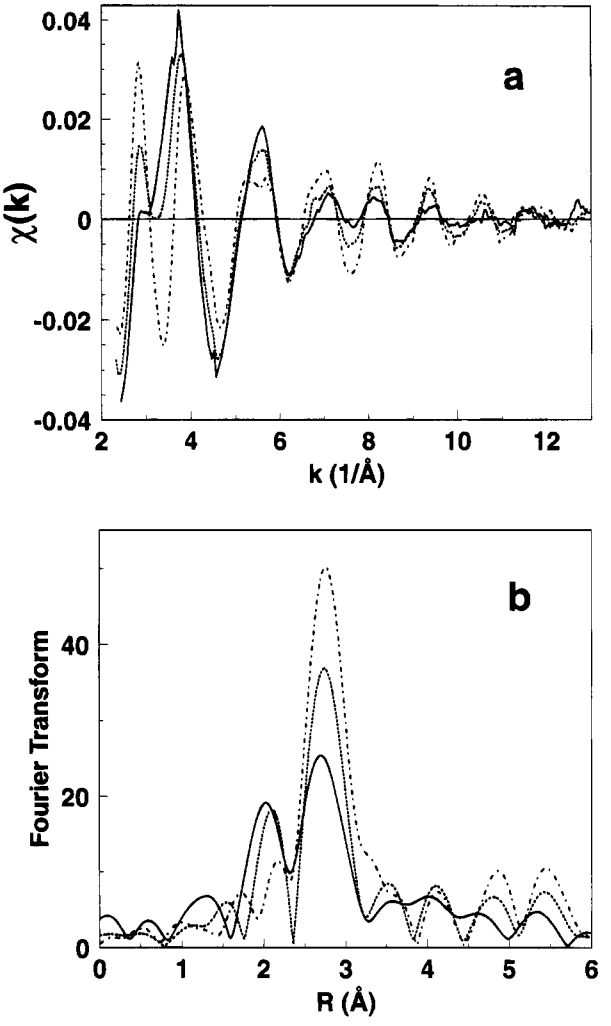

Figure 6. (a) EXAFS spectra of samples DECH180 (solid line), DECH200 (dotted line), and DECH350 (dashed-dotted line). (b) Fourier transform (magnitude) [k^3, Δk = 3.1 − 11.5 Å^{-1}, Pt−Pt phase and amplitude corrected] of EXAFS data of samples DECH180 (solid line), DECH200 (dotted line), and DECH350 (dashed-dotted line).

corresponding to higher Pt−Pt coordination shells in bulk platinum metal (Pt−Pt_2 at 3.92 Å, Pt−Pt_3 at 4.80 Å, and Pt−Pt_4 at 5.54 Å).[28]

The presence of both low Z (Pt−N and/or Pt−O) and high Z contributions (Pt−Pt) in the DECH180 sample can be further demonstrated by applying a k^1-weighted Fourier transform (making the Fourier transform also sensitive to the low Z elements). Figure 7 displays a Pt−Pt phase and amplitude-corrected k^1 weighted Fourier transform of the DECH180 sample (solid line) and Pt foil (dashed line). The main peak in both Fourier transforms is scaled to 1. A comparison of both the magnitude and the imaginary part of the Fourier transform between $1 < R < 2.5$ Å of the DECH180 sample and of the Pt foil demonstrates the presence of a Pt−N and/or Pt−O coordination besides the Pt−Pt bonds in the DECH180 sample. Additionally, the Pt−Pt_2 peak at 3.92 Å, together with another contribution, can be detected in the range $3 < R < 4$ Å for this sample.

The Fourier transforms of the raw data of the samples DECH180, DECH200, and DECH350 were Fourier filtered (see Table 2). The value of the weight factor of the forward Fourier transform was chosen to get an optimum separation between the Pt−Pt_2 and higher shell contributions for DECH180 and DECH200. The Fourier transform of the DECH350 sample was filtered to include the Pt−Pt_4 shell. The isolated EXAFS spectra were fitted with different structural models. Details of the fit procedures (fit ranges in k space, the number of independent points, N_{indp}, the degrees of freedom, ν, and the goodness of the fit, ϵ_ν^2) are given in Table 2. The final results of the EXAFS data analysis of DECH180, DECH200, and DECH350 are presented in Table 3. As can be seen there, submitting the sample in the EXAFS cell to reduction under H_2 at 180 °C for 15 min produces a decrease in the coordination number for Pt^{2+}−L (L = N, O, ≃2.00 Å), the appearance of Pt−Pt bonds at 2.76 and 3.94 Å, and two new Pt−O distances at 2.70 and 3.84 Å, attributed to the metal−support interface.

Parts a and b of Figure 8 include comparative plots of the best fit and isolated EXAFS data for sample DECH180 in k and r space, respectively. To show the relative intensities of the contributions from the interface in this spectrum as well as the quality of the fits, comparative plots of both interfacial shells are included in Figure 8c−e. The difference files containing the separate interfacial platinum oxygen contributions, Pt−O_{L1} = isolated EXAFS − (Pt−L + Pt−O_{L2} + Pt−Pt_1 + Pt−Pt_2) and Pt−O_{L2} = isolated EXAFS − (Pt−L + Pt−O_{L1} + Pt−Pt_1 + Pt−Pt_2), are displayed in k and r space in Figure 8c,d and Figure 8e,f, respectively. The estimated level of the noise amplitude in the raw EXAFS spectrum of the DECH180 sample amounts to 0.002. This noise level is indicated in the difference files (these files are based upon a Fourier filtered EXAFS spectrum) and is given in parts c and e of Figure 8 by two lines with a positive and negative amplitude of 0.001, respectively. With the current version of the EXAFS Data Analysis Program

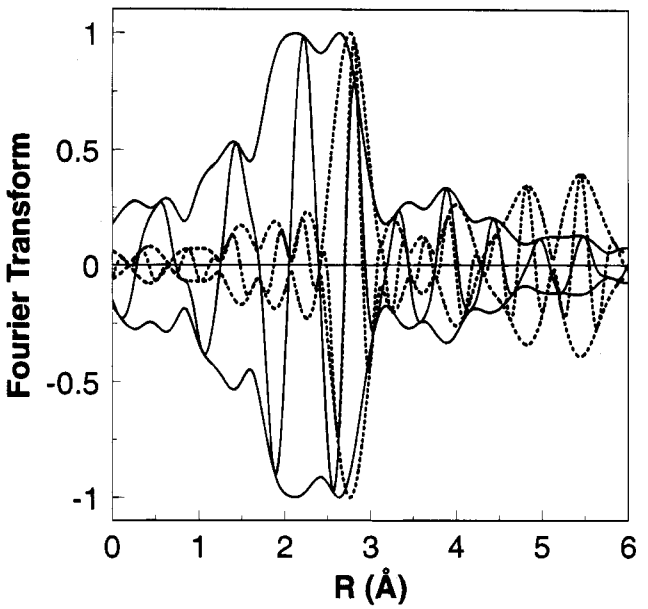

Figure 7. Fourier transform [k^1, Δk = 3.5 − 12 Å^{-1}, Pt−Pt phase and amplitude corrected] of EXAFS spectrum of sample DECH180 (solid line) and Pt foil (dashed line). The latter is scaled to match the amplitude of the former.

(XDAP), the maximum number of parameters that could be kept free during the fitting procedure and for which it was possible to calculate the standard deviations was 16. Taking into account that Pt−Pt_1 and Pt−Pt_2 shells have well-known parameters because they have been fitted many other times,[10−14] we considered the coordination distances and inner potential values ΔE_0 of these shells as fixed (=known parameters) during the calculation of the limits of accuracy, although these four parameters were optimized during the fitting procedure.

Treating under hydrogen at 200 °C (DECH200) produces a further decrease in the coordination number of the Pt^{2+}−N(O) bonds, as well as an increase in the number of neighbors for the first and second Pt−Pt shells. The contribution from the metal−support interface in this sample was too small to allow a reliable analysis. As shown in Table 3, the reduction in H_2 at 350 °C (DECH350) induces an increase in the coordination number for Pt−Pt_1 and Pt−Pt_2 shells as well as the appearance of the third and fourth metal−metal shell at 4.79 and 5.52 Å. The atoms in the fourth shell are shadowed by the atoms in the first shell, resulting in multiple scattering effects. Consequently, the EXAFS signal of this shell is amplified, and an additional amplitude factor has to be introduced. This shell has therefore phase and amplitude functions which differ from the ones of a normal Pt−Pt absorber−backscatterer pair. The fabrication of the reference Pt−Pt_4 has been extensively described in ref 10. Also in this sample the contributions of the metal−support interface were too small to allow a reliable analysis.

The raw EXAFS data of the R350 and OR350 samples are displayed in Figure 9a. Direct reduction in H_2 at 350 °C (R350) of the $[Pt(NH_3)_4](OH)_2$ precursor produces much larger platinum crystallites, whereas calcination before reduction (OR350) leads to smaller platinum particles in comparison with the results obtained from the "slow" decomposition process. This can be seen in Figure 9b, which shows the k^3-weighted Fourier transform (Pt−Pt phase and amplitude corrected) of the EXAFS data obtained from the R350 and OR350 samples together with the same type of Fourier transform for the DECH350 sample. The data quality of the OR350 sample is very good; the noise amplitude is estimated to be 0.001. Figure 10 shows a k^1-weighted Fourier transform (corrected for the Pt−Pt phase and amplitude) of the EXAFS data obtained from the OR350 sample together with the same kind of transform of the spectrum obtained from the platinum foil. Both Fourier transforms are normalized and scaled to one at the first shell Pt−Pt peak. The detectable differences between both transforms for $1 < R < 2.5$ Å are due to the presence of low Z scatters in the EXAFS of the OR350 sample.

The Fourier transform of the EXAFS of the OR350 sample was filtered to include the Pt−Pt_2 shell, whereas the isolated EXAFS of the R350 sample comprises the first four Pt−Pt shells. The results of the full analysis of the OR350 and R350 samples are given in Tables 2 and 3. In sample OR350 a new Pt−O_s shell can be detected, already observed in other supported platinum catalysts treated under hydrogen at higher temperatures.[13,14] In parts a and b of Figure 11 the best fit and isolated EXAFS data for OR350 sample are plotted in k and r space, respectively. Parts c and d of Figure 11 contains the difference file (Pt−O_S + Pt−O_{L1} + Pt−Pt_2 = isolated EXAFS − Pt−Pt_1) obtained from the analysis of the EXAFS spectrum of the OR350 sample in k and r space, respectively. The noise level of the raw EXAFS spectrum is indicated in Figure 11c.

Discussion

Hydrogen Consuming Processes. The process showing a maximum at 315 °C (peak I in the TPR diagram) can be assigned to the main reduction. The integrated area under this peak corresponds to a hydrogen consumption $H_2/Pt = 0.85$. A similar peak has been detected by Laiyuan et al. using a heating rate of 12 °C/min (similar to our heating rate of 10 °C/min) when reducing a chlorinated calcined Pt/γ-Al_2O_3 sample.[37] Hilbrig et al.,[38] using a smaller heating rate (5 °C/min), observed this peak shifted to 275 °C. The amount of hydrogen consumed in our system means nearly two hydrogen atoms for each Pt^{n+} ions, thus indicating that the ammine complex reduction process involves the reaction $Pt^{2+} \rightarrow Pt^0$. The lack of hydrogen consumption to reach the stoichiometric ratio $H_2/Pt = 1.0$ can be due to a partial reduction of the ammine complex while flowing hydrogen at room temperature prior to the TPR experiment.

This reduction process is consistent with the recorded changes in the white line intensities (see Figure 3b). As observed by other authors,[39] when studying bulk platinous compounds (Pt, Pt^{2+}, and Pt^{4+}), white line intensities are a reliable indication of changes in Pt oxidation state. However, monitoring of the white line in this study is not a suitable method to establish quantitatively changes since the intensities of white lines in L-edges reflect two separate processes in the catalyst: variation in the metal particle size and variations in Pt^{n+}/Pt (n = 2, 4) ratio.[40] Although the second process determines to a higher degree the intensity of the white line, the first one can be important in supported metals in highly dispersed state.[41] An extra complication arises from the presence of chemisorbed hydrogen which influences the intensity of the white line.[32]

Once the platinum ions have been reduced, the second peak (peak II, $H_2/Pt = 0.32$, maximum at 465 °C), observed as well by Laiyuan at a similar temperature,[37] can be assigned to an activated hydrogen adsorption process. The third, negative peak ($H_2/Pt = 0.43$, maximum at 550 °C) corresponds to an activated hydrogen desorption. Both processes are strongly related and have been the subject of many studies. Thus, peak III has been recently observed by Primet et al.[3] within the temperature range 450−615 °C and has been associated with hydrogen strongly held on platinum. It was the first detection by Menon et al. that suggested that hydrogen desorbed at this temperature could be located not only on the topmost surface layer but also in a

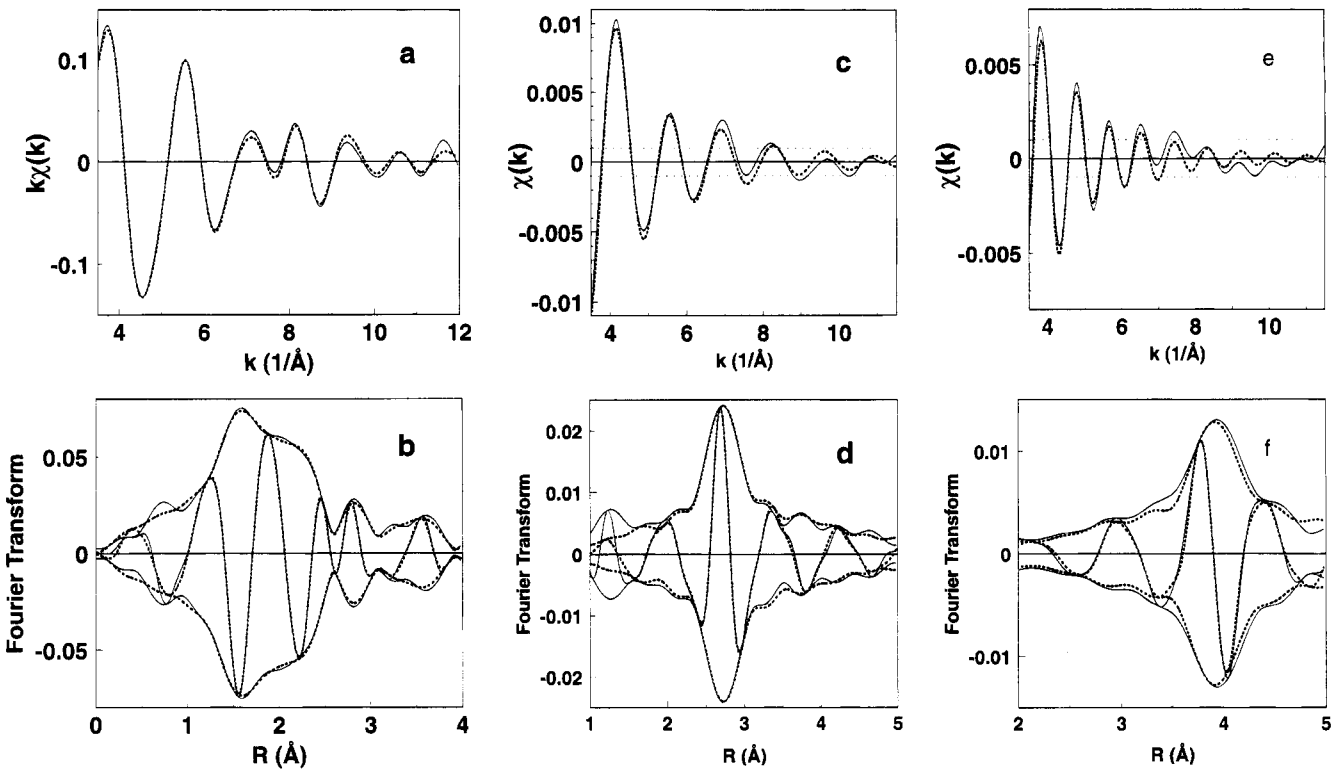

Figure 8. Data analysis results for DECH180: (a) isolated EXAFS (solid line) and best fit (dotted line); (b) Fourier transform [k^1, Δk = 3.5 − 12.5 Å^{-1}] of spectra shown in a; (c) Pt−O_{L1} EXAFS calculated with best-fit parameters (dotted line) and difference file [isolated EXAFS − (Pt^{2+}−N + Pt−Pt_1 + Pt−Pt_2 + Pt−O_{L2})] (solid line); (d) Fourier transform (k^1, Δk = 3.5 − 12.5 Å^{-1}, Pt−O phase corrected) of spectra shown in c; (e) Pt−O_{L2} EXAFS calculated with best-fit parameters (dotted line) and difference file [isolated EXAFS − (Pt^{2+}−N + Pt−Pt_1 + Pt−Pt_2 + Pt−O_{L1})] (solid line); (f) Fourier transform (k^1, Δk = 3.5 − 12.5 Å^{-1}, Pt−O phase-corrected) of spectra shown in e. Estimated noise level in raw EXAFS data of the DECH180 sample is given with a dashed line in Figure 9c,e.

few subsurface layers of platinum.[2] A "high-temperature hydrogen", observed on small platinum particles after hydrogen treatment at 723 K by Rochefort et al.,[42] has been reported to cause a decrease in the rate of methylcyclohexene dehydrogenation, confirming the autoinhibition process mentioned by Menon for alumina-supported platinum catalyst. Recently, this activated hydrogen desorption process has been related (i) to the release of the interfacial hydrogen located between the platinum atoms and support oxide surface and responsible for the Pt^0−O_{L1} bond at 2.7 Å and (ii) to spillover hydrogen.[13,14]

Ammonia Evolution. The study of the MS data indicates that ammine complex disruption, ammonia evolution, and Pt^{2+} reduction are three separate processes that do not take place simultaneously. According to EXAFS results, disruption of the ammine complex—monitored by the decrease of Pt^{2+}−N coordination number—is a process that starts during the drying treatment and is accomplished at the beginning of the reduction process. From MS data it can be inferred that ammonia evolution takes place during the reduction treatment above 300 °C, when the metal reduction process is nearly fulfilled in the EXAFS cell. A reasonable explanation for the MS data is that during the drying and the reduction treatments, Pt^{2+}−N bonds break apart and ammonia ligands are free to adsorb on the acid sites of alumina surface. After this step, ammonia molecules remain on the alumina surface until the temperature is high enough to allow desorption from the strongly acid sites.[35]

Geometrical Structure of the Samples. *1. HE120 Sample: Impregnated and Dried.* The best fit for this sample includes two shells corresponding to unreduced platinum, the first one assigned to Pt^{2+}−N bonds at 2.03 Å and the second to Pt^{2+}−O at 2.00 Å. The first distance is similar to that found for species $[Pt(NH_3)_4]^{2+}$ in the Magnus−Green salt in solid state[28] and in water solution[43] and is within the range of Pt−N bond distances in square planar oxo−ammine complexes, 2.03−2.09 Å,[44] and in $[Pt(en)_2]^{2+}$ (en = $H_2NCH_2CH_2NH_2$), 2.04 Å.[45] The second distance is similar to the values found in PtO and PtO_2.[28] The total coordination number is three. Since the species involved in the impregnation process is $[Pt(NH_3)_4]^{2+}$, one can anticipate finding a coordination number of four around Pt^{2+} ions in the dried sample or, eventually, of five if one water molecule/hydroxyl group is present as an axial ligand, as found by Kraus et al. by SCF calculations.[43] The total coordination number of three for the first shell, as found from EXAFS data analysis, is much lower. It implies that the initial square planar complex undergoes some structural changes during the drying treatment under helium atmosphere at 120 °C, producing a decrease in the coordination number. This structural change can be explained by the formation of platinous oxydiammine [Pt-$(NH_3)_2O$] as found by Reiset[46] by heating the tetrammine hydroxide at 110 °C:[47,48]

$$[Pt(NH_3)_4](OH)_2 \rightarrow [Pt(NH_3)_2O] + H_2O + 2NH_3$$

Alternatively, Dalla Betta and Boudart proposed in 1972 the formation of a neutral mobile hydride in the first stages (below 200 °C) of the reduction of $[Pt(NH_3)_4](OH)_2$, supported on zeolite:[23]

$$[Pt(NH_3)_4]^{2+} + 2H_2 \rightarrow [Pt(NH_3)_2H_2]$$

to account for the low dispersion obtained in the uncalcined sample.

Since our sample was heated at 120 °C under He and the coordination numbers for the Pt−O and Pt−N bonds are one and two, respectively, our findings can only be explained on the basis of the first reaction. Although the low coordination

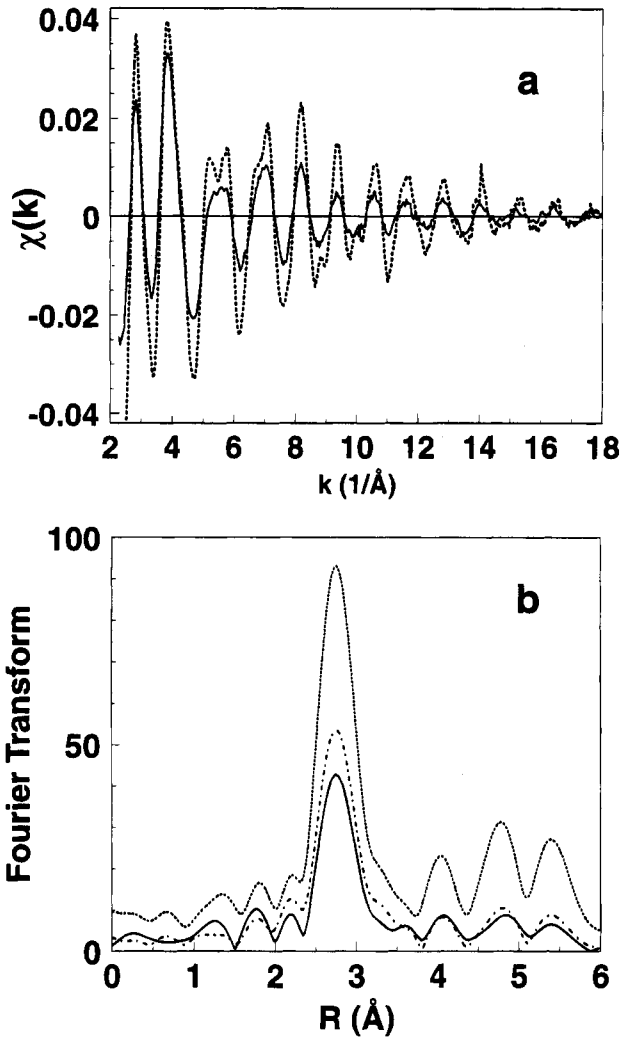

Figure 9. (a) EXAFS spectra of samples OR350 (solid line) and R350 (dotted line). (b) Fourier transform (magnitude) [k^3, $\Delta k = 3.1 - 11.5$ Å^{-1}, Pt−Pt phase and amplitude corrected] of EXAFS data of OR350 (solid line), R350 (dotted line), and for comparison DECH350 (dashed dotted line).

number is not usual in transition metal complexes and the dissociative mode of activation of square planar complexes is a rarity, the existence of such 3-fold coordinated species has been described as intermediate in a dissociative mechanism for ligand exchange in Pt^{2+} square planar complexes.[49]

Our results are not compatible with the proposal made by Dalla Betta and Boudart; the sample has not been submitted to treatment under hydrogen, and the total coordination number would be two, because hydrogen cannot be detected since the backscattering amplitude is too low. Since the oxydiammine $[Pt(NH_3)_2O]$ complex is neutral, it will have a high mobility thus allowing the sintering of the metal particles. This can nicely explain the low metal dispersion of the samples which were not calcined before reduction.

2. Samples DECH180, DECH200, DECH350: Decomposed and Reduced Species. The decrease in the coordination number of bonds at 2.00−2.03 Å indicates the decrease in the concentration of the oxidized species, Pt^{2+}, during the reduction treatment. Nevertheless, the increase in the coordination number for Pt−Pt bonds does not indicate unambiguously the increase in metal particle size because the Pt−Pt coordination number obtained from the EXAFS analysis is averaged over all Pt atoms in the sample, i.e., in the metallic state as well as in the oxidic phase. In this case EXAFS coordination parameters have to be corrected taking into account the fraction of the metal

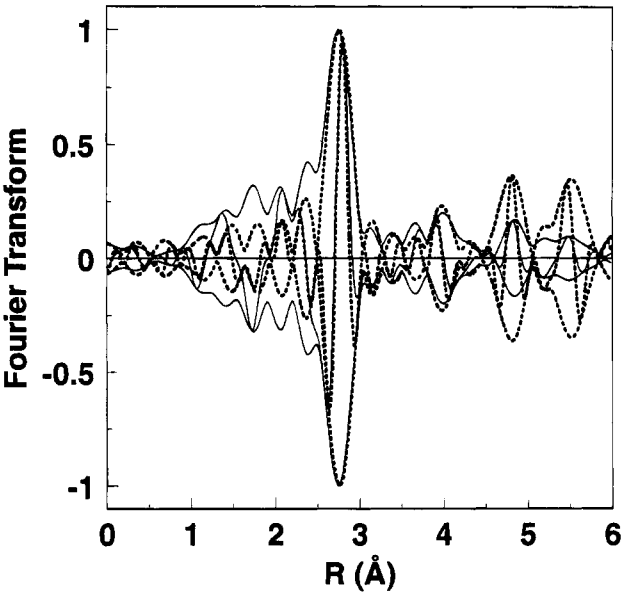

Figure 10. Fourier transform [k^1, $\Delta k = 3.1 - 14.3$ Å^{-1}, Pt−Pt phase and amplitude corrected] of EXAFS spectrum of sample OR350 (solid line) and of Pt foil (dashed line). The latter is scaled to match the amplitude of the former.

oxidized.[50] As it has been discussed before, this fraction cannot be calculated reliably in our system; direct extrapolation of the conclusions from the TPR profile cannot be made since experimental conditions are different, and changes in the white line involve several processes on top of the metal reduction. Alternatively, this information can be found in the coordination number of the Pt−O bonds from the interface as well as in the appearance of higher Pt−Pt shells.

Firstly, the appearance of $Pt-Pt_2$ and $Pt-Pt_3$ shells indicates unambiguously the increase of metal particle size in samples DECH200 and DECH350 as compared to that in sample DECH180. Secondly, the coordination numbers for the different Pt−Pt coordination shells derived from the analysis of the EXAFS data of DECH350, R350, and OR350 allow a quantification of metal particle size. Samples DECH180 and DECH200 have not been considered because platinum is not fully reduced and coordination numbers for Pt−Pt shells are fractional. To carry out a reliable calculation of this value, some information is needed about the morphology of the metal particles. EXAFS can provide this information; in particular it allows distinction between three- and two-dimensional crystallites. Thus, the existence of second metal−metal shells at 3.94 Å in all samples discards the formation of bidimensional particles. With this knowledge and the assumption of the existence of fcc spherical particles, from model calculations, the behavior of the average coordination number as a function of the number of atoms in the particle for the first three shells can be derived.[10] We have used these calculations to estimate the number of atoms in the particle from the coordination number of metal−metal shells in the fully reduced samples. The number of atoms in the particle and the particle diameter have been estimated independently for each shell in samples DECH350, R350, and OR350, and the results are included in Table 4. It has to be taken into account that, due to its smaller intensity, the accuracy in coordination number obtained from the second shell is smaller than the values obtained from the first and third shell.

From the examination of Table 4 we can extract two conclusions. The first is that the direct reduction yields the biggest metal particles, while oxidizing treatment prior to reduction produces the smallest metal particle size. To reliably obtain these values for both samples, the first (and third) Pt−

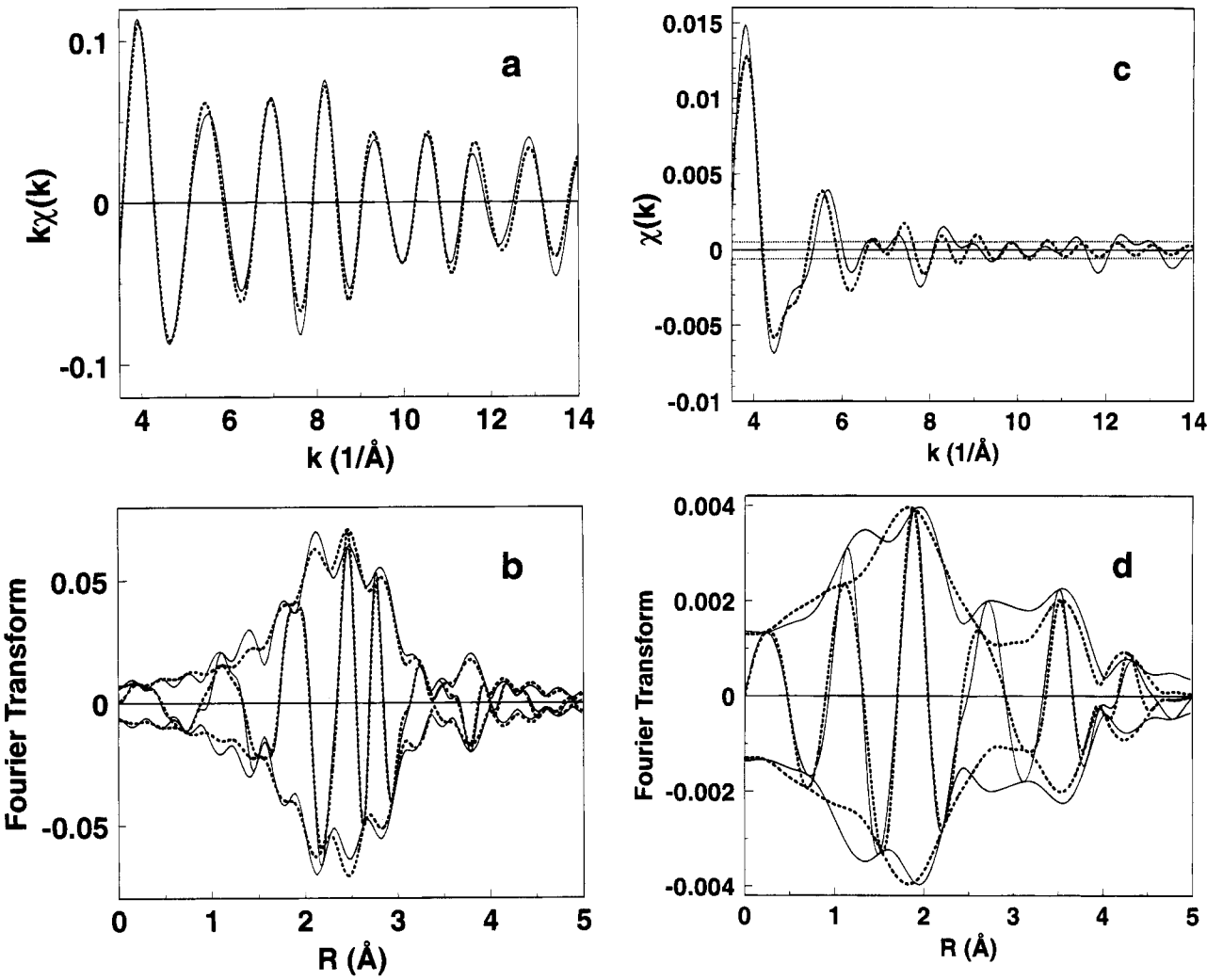

Figure 11. Data-analysis results for OR350: (a) isolated EXAFS (solid line) and best fit (dotted line); (b) Fourier transform [k^1, Δk = 3.5 − 13.5 Å^{-1}] of spectra shown in a; (c) Pt−O_S + Pt−O_{L1} + Pt−Pt_2 EXAFS calculated with best-fit parameters (dotted line) and difference file (isolated EXAFS − (Pt−Pt_1) (solid line); (d) Fourier transform (k^0, Δk = 3.5 − 10.0 Å^{-1}) of spectra shown in c.

TABLE 4: Coordination Numbers, Number of Atoms per Particle, and Particle Diameter for Fully Reduced Samples

	DECH350			R350			OR350		
shell	N_{Pt-Pt}	n_{atoms}	D (Å)	N_{Pt-Pt}	n_{atoms}	D (Å)	N_{Pt-Pt}	n_{atoms}	D (Å)
1	7.2	40	13	10.1	650	35	5.5	14	9
2	2.8	40	13	4.4	360	27	2.0	19	11
3	8.8	40	13	17.5	650	35			

Pt shells can be used. A sample decomposed and reduced at 350 °C is an intermediate situation; metal particles are considerably smaller those in the directly reduced sample but larger than those in the oxidized and reduced sample. Moreover, the fact that the metal particle size deduced from the three shells is exactly the same is an indication of homogeneous particle size and shape as well as a very consistent fit. All these conclusions are confirmed by the values of another parameter included in Table 3: the Debye−Waller factor. Since they are an indication of local order, they should decrease as metal particle size increases. As expected, Debye−Waller factors for Pt−Pt_1, Pt−Pt_2, and Pt−Pt_3 shells present the smallest values in sample R350. Since there is an increase in coordination number for the same contributions, a coupling between these two parameters is discarded.

The second conclusion is that the beneficial effect of calcination prior to reduction, already observed by several authors when preparing supported platinum catalysts using [Pt-$(NH_3)_4$]$(OH)_2$ as precursor,[10,23] can be explained now in light of the results here presented. As shown before, the decomposition process in nonoxidizing environments generates oxydiammineplatinous complex, [$Pt(NH_3)_2O$], which, being neutral, has a very high mobility. A neutral hydride complex, [$Pt(NH_3)_2H_2$], was already proposed by Dalla Betta and Boudart to explain the lowest dispersion obtained in Pt−zeolite samples prepared by direct reduction of [$Pt(NH_3)_4$]$(OH)_2$. We support their hypothesis of the neutral complex, but, on the basis of the EXAFS analysis of sample DECHE120, the neutral complex is the oxydiammine instead of the dihydride.

The smallest particle size of the decomposed and reduced sample when compared with the directly reduced sample can be attributed to the other factor determining metal particle growth: water vapor pressure during reduction.[18,19] The drying treatment under helium and the slow reduction step in sample DECH350 should have kept the water pressure at a much lower level than that in the directly reduced samples. Consequently, platinum particles are smaller in this sample.

More research is needed to generalize and to extrapolate the preparation conditions using [$Pt(NH_3)_4$]$(OH)_2$ as a precursor for creating highly dispersed platinum particles onto other supports different from γ-Al_2O_3. For instance, extremely small platinum clusters dispersed onto LTL zeolite can be obtained by impregnation followed by drying at 120 °C and direct reduction in hydrogen using a high gas flow (>100 mL/min).[11,13,14] Calcination at low temperature (~280 °C) followed by reduction

also leads to a high dispersion in the same system.[24] It is probable that the pore structure and morphology of the LTL zeolite decrease the mobility of the neutral $[Pt(NH_3)_2O]$ complex implying that the pretreatment conditions can be slightly different for the LTL support.

Bazin et al.[9] followed the decomposition of the H_2PtCl_6 precursor onto γ-Al_2O_3 using the dispersive EXAFS technique. They claimed to detect, during the decomposition of the precursor, a "long Pt−Pt bond" at 2.85 Å. In all the samples studied in this paper no trace of a Pt−Pt bond at 2.85 Å has been detected. Nevertheless, some evidence of direct Pt−Pt bonds at values different from that of the bulk metal has been reported to occur in several coordination compounds. For instance, in tetranuclear platinum complexes Pt−Pt distances in the range 2.57−2.60 Å, slightly shorter than those in the metal, have been observed by Betz et al.[51] Longer distances have been observed in "platin blaus" complexes, where the average oxidation state of Pt is 2.25, each platinum ion is coordinated by two nitrogen and two oxygen atoms, and Pt−Pt distances range from 2.78 to 2.93 Å.[52] In these complexes, the highest Pt−Pt coordination distance is determined by Columbic repulsion between equally charged ions. In fully reduced systems the only coherent distances reported up to now are those of the bulk metal. However, the "long Pt−Pt bond" derived by Bazin et al.[9] from their EXAFS data analysis can be related to a partially reduced system, as in "platin blaus" mentioned above. Alternatively, the detection of the "long Pt−Pt bond" could be due to the use of "normal" Fourier transforms for assigning peaks in the EXAFS data. Owing to the nonlinearity of the phase shift and the k dependence of the backscattering amplitude of the Pt−Pt absorber−backscatterer pair, a single Pt−Pt contribution gives rise to three distinguishable peaks in a normal Fourier transform.[30] The side lobes at the high R side of the triple peak of the single Pt−Pt contribution occur at about the distance claimed by Bazin et al. to be caused by the presence of a long Pt−Pt distance. Therefore, the long Pt−Pt distance may be caused by an artifact in the EXAFS data analysis method.

Structure of the Metal−Support Interface. The structure of the interface is characterized by two Pt−O contributions at 2.75 and 3.85 Å which can be clearly detected only when the Pt−Pt contribution is still small (DECH180) and the signal to noise is sufficiently high (OR350). This can be appreciated in Figure 8c−f and Figure 11c where the metal−support contributions have been plotted in k space together with the maximum noise level of the original raw EXAFS data. The metal−support contributions in both samples have comparable intensities, and in this way the structure of the interface can be studied reliably. The experimental conditions for which a Pt−O coordination at around 2.7 Å can be created in the metal−support interface of LTL supported platinum particles have been extensively investigated by Vaarkamp et al.[14] and Miller et al.[13] A combination of TPD and EXAFS experiments shows that direct reduction at low temperature (≤300 °C) creates hydrogen in the metal−support interface, giving rise to the detection of a long Pt−O distance. During the consecutive reduction at high temperatures (≥500 °C) the interfacial hydrogen is released from the metal−support resulting in a direct contact of the interfacial platinum atoms with the support. As a consequence, the Pt−O distance in the metal−support is found to be much shorter: 2.2 Å. At intermediate temperatures both types of distances can be detected,[14] as found for the Pt/γ-Al_2O_3 catalysts OR350 studied in this paper. A similar contribution has been detected by Purnell et al.[53] in the study of the growth of platinum particles on MgO and by Chang et al.[54] when studying the decomposition of mononuclear rhenium clusters onto the same support.[55] Both observed that this Pt−O_s distance did not change with variation in the treatment conditions, a result consistent with the literature reporting that the short metal−oxygen distance observed for many oxide-supported metals is generally in the range 2.0−2.2 Å.[54] Moreover, this metal−oxygen distance in organometallic analogs is insensitive to the metal oxidation state.[55]

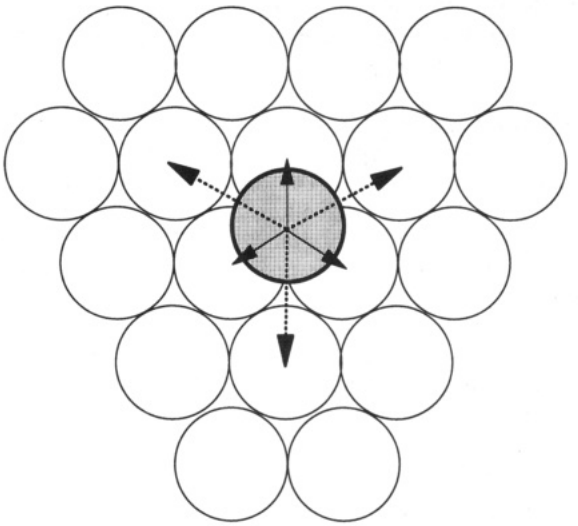

Figure 12. Simplified structural model of metal−support interface. Open circles are oxygen ions of the [111] surface layer of the γ-Al_2O_3 support. The platinum metal particle is assumed to have a [111] epitaxy in the interface with the top oxygen of the support adapted to the Pt−Pt distances of the (interfacial) platinum atoms. The interfacial platinum atoms (hatched circle) have a first shell oxygen coordination (Pt−O_{L1}) at 2.7 Å (solid arrow) and second shell oxygen coordination (Pt−O_{L2}) at 3.86 Å (dotted arrow).

Reduction at high temperatures causes both the disappearance of the long Pt−O distance and the removal of the spillover hydrogen[13,14] from the support. Moreover, the hydrogen chemisorption[56] and catalytic properties[57] of supported platinum catalysts are strongly influenced by the hydrogen pretreatment procedure.

The detection of a Pt−O contribution at 3.8 Å as analyzed in the EXAFS data of DECH180 is a consequence of the presence of a Pt−O coordination at 2.7 Å. The (fractional) coordination number of this "second shell" long Pt−O distance is similar to that found for the "first shell" long Pt−O distance. A structural model which incorporates the second shell Pt−O distance based upon a first shell Pt−O distance at 2.7 Å is given in Figure 12. This structural model assumes a [111] epitaxy in the interface, which is possible if the distance between the top oxygen atoms of the support in the [111] plane is adapted to the Pt−Pt distance of the interfacial platinum atoms. This structural model may describe the structure of the metal−support interface after treatment in hydrogen at 180 °C. It cannot be excluded that after high temperature reduction treatments a different epitaxy and structure exist in the metal−support interface.

Conclusions

When $[Pt(NH_3)_4](OH)_2$ is used as a precursor to generate small platinum particles dispersed onto γ-Al_2O_3, calcination before reduction is a prerequisite. In the dried, uncalcined samples the platinum entities undergoing reduction are the oxydiammine complexes $[Pt(NH_3)_2O]$. Calcination avoids the formation of this neutral, and therefore mobile, complex. After treatment under flowing hydrogen at 180 °C platinum metal particles are formed having a size that allows reliable detection

with the EXAFS technique. The metal−support interface in the supported platinum particles is characterized by two Pt−O distances at 2.75 and 3.85 Å.

Acknowledgment. Thanks are due to Dr. P. Malet for recording and discussing TPR and to Dr. M. Vaarkamp for help with the fitting program. The SRS (Daresbury Laboratory, U.K.) is acknowledged for allocation of beam time, and the Spanish DGICYT (Project Number PB92-0671) and Dutch NWO are acknowledged for financial support and supplying grants for traveling.

Supplementary Material Available: Figures showing EXAFS spectra, Fourier transforms, and fits (5 pages). Ordering information is given on any current masthead page.

References and Notes

(1) Foger, K. *Catalysis Science and Technology*; Anderson, J. R., Boudart, M. Springer Verlag: Berlin, 1984; Chapter 4.
(2) Menon, P. G.; Froment, G. F. *Appl. Catal.* **1981**, *1*, 31.
(3) Levy, P. J.; Primet, M. *Appl. Catal.* **1991**, *70*, 263.
(4) Marchese, L.; Boccuti, M. R.; Coluccio, S.; Lavagnino, S.; Zecchina, A.; Bonneviot, L.; Che, M. *Structure and Reactivity of Surfaces*; Morterra, C., Zecchina, A., Costa, G., Eds.; Elsevier: Amsterdam, 1989; p 653.
(5) Fritsch, A.; Légaré, P. *Surf. Sci.* **1987**, *184*, L355.
(6) Smith, D. J.; White, D.; Baird, T.; Fryer, J. R. *J. Catal.*, **1983**, *81*, 107.
(7) Joyner, R. W. *J. Chem. Soc., Faraday Trans. 1* **1980**, *76*, 357.
(8) Lytle, F. W.; Greegor, R. B.; Marques, E. C.; Sandstrom, D. R.; Via, G. H.; Sinfelt, J. H. *J. Catal.* **1985**, *95*, 546.
(9) Bazin, D.; Dexpert, H.; Bournonville, J. P.; Lynch, J. *J. Catal.* **1990**, *123*, 86.
(10) Kampers, F. W. H.; Engelen, C. W. R.; Van Hooff, J. H. C.; Koningsberger, D. C. *J. Phys. Chem.* **1990**, *94*, 8574.
(11) Vaarkamp, M.; Van Grondelle, J.; Koningsberger, D. C.; Miller, J. T.; Sajkowski, D. J.; Modica, F. S.; Lane, G. S.; Gates, B. C. *Catal. Lett.* **1990**, *6*, 369.
(12) Samant, M. G.; Boudart, M. *J. Phys. Chem.* **1991**, *95*, 4070.
(13) Miller, J. T.; Meyers, B. L.; Modica, F. S.; Lane G. S.; Vaarkamp, M.; Koningsberger, D. C. *J. Catal.* **1993**, *143*, 395.
(14) Vaarkamp, M.; Modica, F. S.; Miller, J. T.; Koningsberger, D. C. *J. Catal.* **1993**, *144*, 611.
(15) Ardiles, D. R.; De Miguel, S. R.; Castro, A. A.; Scelza, A. O. *Appl. Catal.* **1986**, *24*, 175.
(16) De Miguel, S. R.; Scelza, O. A.; Castro, A. A.; Baronetti, G. T.; Ardiles, D. R.; Parera, J. M. *Appl. Catal.* **1984**, *99*, 309.
(17) Martens, J. H. A. Ph.D. Thesis, Eindhoven University, The Netherlands, 1988.
(18) Malet, P.; Munuera, G.; Caballero, A. *J. Catal.* **1989**, *115*, 567.
(19) Margitfalvi, J.; Kern-Talas, E.; Szedlacsek, P. *J. Catal.* **1985**, *92*, 193.
(20) Bertolacini, R. J.; Kim, D. K. U.S. Patent 4,134,823, 1979; *Chem. Abstr.* **1979**, *91*, 6008.
(21) Van Tiep, L.; Bureau-Tardy, M.; Bugli, G.; Djega-Mariadassou, G.; Che, M.; Bond, G. C. *J. Catal.* **1986**, *9*, 449.
(22) Kip, B. J.; Dirne, F. W. A.; Van Grondelle, J.; Prins, R. *Appl. Catal.* **1986**, *25*, 43.
(23) Dalla Betta, R. A.; Boudart, M. *Proceedings of the 5th International Congress on Catalysis*; North Holland: New York, 1972; Vol. 2 p 1329.
(24) Lane, G. S.; Modica, F. S.; Miller, J. T. *J. Catal.* **1991**, *129*, 145.
(25) Kampers, F. W. H.; Maas, T. M. J.; Van Grondelle, J.; Brinkgreve, P.; Koningsberger, D. C. *Rev. Sci. Instrum.* **1989**, *60*, 2635.
(26) Cook, J. W., Jr.; Sayers, D. E. *J. Appl. Phys.* **1981**, *52*, 5024.
(27) Van Zon, J. B. A. D.; Koningsberger, D. C.; Van Blik, H. F. J.; Sayers, D. E. *J. Chem. Phys.* **1985**, *82*, 5742.
(28) Wyckoff, R. W. G. *Crystal Structures*; Interscience: New York, 1974.
(29) Trömel, M.; Lupprich, E. *Z. Anorg. Allg. Chem.* **1975**, *414*, 160.
(30) Koningsberger, D. C. Stereochemistry and Electronic Structure. XAFS Spectroscopy: Data-Analysis and Applications. In *Physics and Chemistry of Solids. Hercules Course*; Baruchel, J., Hodeau, J. L., Lehmann, M. S., Regnard, J. R., Schlenker, C., Eds.; Springer Verlag: Berlin, 1993; Vol. II, Chapter X, p 213.
(31) Duivenvoorden, F. B. M.; Koningsberger, D. C.; Uh, Y. S.; Gates, B. C. *J. Am. Chem. Soc.* **1986**, *108*, 6254.
(32) Vaarkamp, M. Ph.D. Thesis, Eindhoven University, The Netherlands, 1993.
(33) Lytle, F. W.; Sayers, D. E.; Stern, E. A. *Physica B* **1988**, *158*, 701.
(34) Knozinger, H.; Ratnasamy, P. *Catal. Sci. Eng.* **1978**, *17* (1), 31.
(35) Berteau, P.; Delmon, B. *Catal. Today* **1989**, *5*, 121.
(36) Pandya, K. I.; Koningsberger, D. C. *Physica B* **1989**, *158*, 386.
(37) Laiyuan, C.; Yuequin, N.; Jingling, Z.; Liwu, L.; Xihui, L. Sen, C. *J. Catal.* **1994**, *145*, 132.
(38) Hilbrig, F.; Michel, C.; Haller, G. *J. Phys. Chem.* **1992**, *96*, 9899.
(39) Lytle, F. W.; Wei, P. S. P.; Greegor, R. B.; Via, G. H.; Sinfelt, J. H. *J. Chem. Phys.* **1979**, *70*, 4849.
(40) Botman, M. J. P.; Den Hartog, A. J.; Ponec, V. *Structure and Reactivity of Surfaces*; Morterra, C., Zecchina, A., Costa, G., Eds.; Elsevier: Amsterdam 1989, p 179.
(41) Meitzner, G.; Via, G. H.; Lytle, F. W.; Sinfelt, J. H. *J. Phys. Chem.* **1992**, *96*, 4960.
(42) - Rochefort, A.; Le Peltier, F.; Boitiaux, J. P. *J. Catal.* **1994**, *145*, 409.
(43) Krauss, M.; Brasch, H.; Miller, K. J. *J. Am. Chem. Soc.* **1988**, *110*, 4517.
(44) Randaschl-Sieber, G.; Schollhron, H.; Thewalt, V.; Lippert, B. *J. Am. Chem. Soc.* **1985**, *107*, 3591.
(45) Teo, B. K.; Eisenberger, P.; Reed, J.; Barton, J. K.; Lipparel, S. J. *J. Am. Chem. Soc.* **1978**, *100*, 3225.
(46) Reiset, J. *Am. Chem. Phys.* **1884**, *11*, 423.
(47) Pascal, P. *Noveau Traité Chimie Minérale*; Masson Editeur: Paris, 1958; Vol. XIX, p 860.
(48) Mellor, J. W. *A Comprehensive Treatise of Inorganic and Theoretical Chemistry*; Longmans Green: London, 1945; Vol. XVI, p 236.
(49) Frey, U; Helm, L.; Merbach, A. E.; Romeo, R. *J. Am. Chem. Soc.* **1989**, *111*, 8161.
(50) Wijnen, P. W. J. G.; Van Zon, F. B. M.; Koningsberger, D. C. *J. Catal.* **1988**, *114*, 463.
(51) Betz, P.; Bino, A. *J. Am. Chem. Soc.* **1988**, *110*, 602.
(52) Sakai, K.; Matsumoto, K. *J. Am. Chem. Soc.* **1989**, *111*, 3074.
(53) Purnell, S. K.; Sanchez, K. M.; Patrini, R.; Chang, J.-R.; Gates, B. C. *J. Phys. Chem.* **1994**, *98*, 1205.
(54) Chang, J. R.; Gron, A.; Honji, K.; Sanchez, K. M.; Gates, B. C. *J. Phys. Chem.* **1991**, *95*, 9944.
(55) Vaarkamp, M.; Modica, F. S.; Miller, J. T.; Koningsberger, D. C. Submitted for publication in *J. Phys. Chem.*
(56) Vaarkamp, M.; Modica, F. S.; Miller, J. T.; Koningsberger, D. C. Submitted for publication in *J. Catal.*

JP942156P